Original Article

Asian Pacific Journal of Tropical Biomedicine

apjtb.org

doi: 10.4103/2221−1691.391156

Impact Factor® 1.7

Luteolin attenuates diabetic nephropathy *via* inhibition of metalloenzymes in rats

R. B. Daude[1], Rajendra Bhadane[2,3,4], J. S. Shah[5]✉

[1]*Department of Pharmacy, Government Polytechnic, Jalgaon−425001, Maharashtra, India*

[2]*Structural Bioinformatics Laboratory, Faculty of Science and Engineering, Biochemistry, Åbo Akademi University, FI−20520 Turku, Finland*

[3]*Pharmaceutical Sciences Laboratory, Faculty of Science and Engineering, Pharmacy, Åbo Akademi University, FI−20520 Turku, Finland*

[4]*Institute of Biomedicine, Research Unit for Infection and Immunity, University of Turku, FI−20520 Turku, Finland*

[5]*Department of Pharmacology, Institute of Pharmacy, Nirma University, Ahmedabad−382481, Gujrat, India*

ABSTRACT

Objective: To investigate the renoprotective effects of luteolin on diabetes in rats.

Methods: One week after administration of streptozotocin 55 mg/kg intraperitoneally, rats were given 25, 50, and 75 mg/kg/day of luteolin orally for another eight weeks. At the end of the experiment, body weight, blood glucose level, biochemical parameters for renal function (serum creatinine, blood urea nitrogen, uric acid, serum albumin, and total protein), kidney histology, matrix metalloproteinase (MMP)-2, MMP-9, and histone deacetylase 2 (HDAC-2) expression, and malondialdehyde, myeloperoxidase, and hydroxyproline content in renal tissue were evaluated. High glucose-induced damage using NRK-52E cell line was studied to evaluate cell viability and metalloenzyme expression. Additionally, *in silico* studies including docking and molecular dynamics simulations were conducted.

Results: MMP-2, MMP-9, and HDAC-2 expressions were significantly increased in high glucose-induced NRK-52E cells and the renal tissue of diabetic rats. However, these changes were reversed by luteolin at the administered doses. Additionally, luteolin significantly reduced oxidative stress, inflammation, and fibrosis, as well as improved biochemical parameters in diabetic rats. Furthermore, luteolin at the examined doses markedly alleviated diabetes-induced histopathological changes in renal tissues.

Conclusions: Luteolin effectively attenuates streptozotocin-induced diabetic nephropathy in rats by inhibiting MMP-2, MMP-9, and HDAC-2 expression, and reducing oxidative stress and inflammation.

KEYWORDS: MMPs; HDAC-2; Luteolin; NRK-52E; Diabetic nephropathy; Docking; Molecular dynamic simulations

1. Introduction

Diabetic nephropathy (DN), a chronic microvascular complication of diabetes mellitus, eventually causes end-stage renal disease. Over the past two decades, there has been a significant increase in the prevalence of DN globally, resulting in a rise in mortality and morbidity rates[1]. The persistent hyperglycemia-induced metabolic changes associated with DN lead to morphologic changes such as glomerular hypertrophy, glomerulosclerosis, tubulointerstitial inflammation, and fibrosis[2]. Diabetic kidney damage can develop despite glucose control and antihypertensive drugs. Therapy options

Significance

Luteolin, a flavonoid, is reported to mitigate risk factors associated with diabetic complications. This study demonstrates the therapeutic efficacy of luteolin in combating streptozotocin-induced diabetic nephropathy in rats. Luteolin targets MMP-2, MMP-9, and HDAC-2 levels in the early stages of the disease, safeguarding glomerular architecture and impeding the progression of the disease. Luteolin also reduces oxidative stress and inflammation, regulates hyperglycemia, and improves kidney function, and renal histoarchitecture. Our study signifies the role of luteolin in an early-stage treatment for diabetic nephropathy by targeting metalloenzymes.

✉To whom correspondence may be addressed. E-mail: Jigna.shah@nirmauni.ac.in

How to cite this article: Daude RB, Bhadane R, Shah JS. Luteolin attenuates diabetic nephropathy *via* inhibition of metalloenzymes in rats. Asian Pac J Trop Biomed 2023; 13(12): 507-520.

Article history: Received 13 June 2023; Revision 8 August 2023; Accepted 10 November 2023; Available online 28 December 2023

for DN encompass renin-angiotensin system blockers, glucagon-like peptide-1 receptor agonists, and sodium-glucose transporter-2 inhibitors[1,2]. However, despite the availability of these therapeutic options, current medications are not entirely effective in treating DN. Understanding the molecular processes underlying DN pathogenesis is crucial for developing more effective treatments with enhanced therapeutic targets and supportive treatments.

Matrix metalloproteinases (MMPs) are zinc-dependent enzymes that continuously degrade and remodel the extracellular matrix (ECM). Two specific MMPs, MMP-2 (72 kD gelatinase A) and MMP-9 (92 kD gelatinase B), degrade key basement membrane components like type Ⅳ collagen, laminin, and fibronectin[3]. Most MMPs are produced as inactive proMMPs, which can be activated by proteinases like plasmin and MT-MMPs. Plasmin is particularly effective in degrading matrix elements and activating latent MMPs. Tissue metalloproteinase inhibitors (TIMPs) can reduce MMP activity through other pathways. MMP substrates can cleave cell adhesion molecules and signaling molecules, including growth factor receptors[4,5]. MMP-2 and MMP-9 expression and activity can be altered in acute and chronic kidney disease[4]. MMP-2 has been shown to promote renal interstitial fibrosis that occurs in DN by promoting the shift of the renal tubular epithelium to the myofibroblastic phenotype[4]. On the other hand, studies have also found that before the onset of microalbuminuria, the concentration of MMP-9 in the urine of diabetics increased, suggesting the involvement of MMP-9 in the development of DN[6]. The progression of the disease is brought about by the simultaneity of events due to persistent hyperglycemia which triggers reactive oxygen species (ROS). Transforming growth factor β1 causes renal epithelial-mesenchymal transition (EMT) by degrading type Ⅳ collagen through MMP-2 overexpression, leading to disease progression[4]. The findings obtained from these studies provide a solid foundation for involvement of MMPs in the progression of DN.

Epigenetic studies have unveiled the crucial involvement of all classes of histone deacetylases (HDACs) in diabetic complications through the modification of histones. The role of HDAC-2 in contributing to the progression of diabetes and its associated complications has been documented[7]. Hyperglycemia causes ROS formation *via* transforming growth factor-1, which activates HDAC-2, thus speeding up the advancement of ECM and EMT in diabetic kidneys[8]. Preliminary evidence suggests targeting HDAC-2 may benefit DN. The recent investigation revealed that early therapy with MMP-2 and MMP-9 inhibitors can restore the glomerular glycocalyx architecture in experimental diabetic animals[4]. Additionally, oxidative stress is known to destroy the endothelial glycocalyx by increasing HDAC activity, which enhances MMP production and decreases TIMP by cleaving syndecan and proteoglycans[9]. The approaches of the above studies may offer a viable solution for DN through early targeting of metalloenzymes and ROS.

Bioflavonoids, including luteolin, have long been studied for their potential pharmacological actions in DN. Several *in vivo* and *in vitro* investigations have shown that luteolin has anti-oxidant, anti-inflammatory, anti-diabetic, anti-allergic, anti-uric acid, and anti-cancer properties with potential therapeutic implications[10]. Recent studies have reported that luteolin, when administered orally, preserves basement membrane filtration function by upregulating NPHS2 protein expression and preventing kidney deterioration by suppressing glomerulosclerosis and maintaining normal glomerular structure[11]. Additionally, luteolin reduces the inflammatory response and oxidative stress through inhibition of the STAT3 pathway, delaying the development of DN[12]. Luteolin also reduces morphological kidney damage and improves renal redox balance by changing the expression of HO-1 and p-Akt, potentially delaying DN[13]. Based on the above findings, luteolin may modulate the oxidative inflammation pathway to reduce persistent hyperglycemia-induced renal consequences, but its effects on metalloenzymes (MMPs and HDAC-2) in DN have yet to be elucidated.

The objective of the present study was to examine the molecular interactions between luteolin, HDAC-2, and MMPs. To achieve this, we employed a structure-based drug design approach, which was then followed by molecular dynamics simulations and an assessment of binding free energy[14] in order to determine whether luteolin can protect against renal dysfunction induced by hyperglycemia and oxidative stress. Additionally, we conducted *in vitro* studies and utilized a streptozotocin-induced rat model of early DN to investigate the effect of luteolin on the protein expression of MMP-2, MMP-9, and HDAC-2, as well as the pathophysiological changes associated with luteolin treatment in rats with DN.

2. Materials and methods

2.1. Chemicals

Streptozotocin (STZ) was obtained from Sigma Chemicals Ltd., Germany, and luteolin was purchased from Santacruz Biotechnology Ltd., Dallas, Texas, USA. All other chemicals required for experiment were purchased from SRL, Mumbai, India. Kits for testing blood glucose (Accu-check Glucometer) and other biochemical parameters were purchased from Erba Diagnostic Mumbai, India. MMP-2 (KLR0315), MMP-9 (KLR0321), and HDAC-2 (KLR1410) ELISA kits were purchased from Krishgen Biosystem, Mumbai, India.

2.2. Animals

Before the initiation of the studies, male Wistar rats, each weighing between 200-250 g (8-10 weeks of age), were acclimatized for two weeks in a standard laboratory setting. Throughout the experimentation, the animals were housed in a room that was properly ventilated, with a rate of 16-18 air changes per hour, and

maintained at a controlled temperature range of 20-24 ℃, relative humidity of 45%-65%, and a light/dark cycle of 12 h. The rats were provided with unrestricted access to feed pellets and clean water.

2.3. Induction and assessment of diabetes

Rats were subjected to an overnight fast before receiving a single intraperitoneal injection of streptozotocin (55 mg/kg), formulated in 0.1 mol/L ice-cold citrate buffer pH 4.5, to induce diabetes. STZ was individually weighed for each animal and administered within 5 min to prevent degradation. Because STZ can cause fatal hypoglycemia due to massive insulin release, rats were given a 10% sucrose solution for 24 h after the STZ injection. One week after the administration of the STZ injection, blood samples were collected from the tail veins of the overnight-deprived rats to confirm the presence of hyperglycemia. The blood glucose levels were measured using a glucometer, and any rats exhibiting blood glucose levels greater than 300 mg/dL were deemed diabetic and included in the study[15].

The diabetic rats were then divided into five groups with six rats in each group: Group Ⅰ: non-diabetic rats were administered sodium carboxymethyl cellulose (Na-CMC) (0.5% *w/v*) in water as a vehicle; Group Ⅱ: diabetes control rats that were given STZ (55 mg/kg *i.p.*) received Na-CMC in water; Group Ⅲ: diabetic rats received luteolin (25 mg/kg *p.o.*) suspended in Na-CMC (0.5% *w/v*); Group Ⅳ: diabetic rats received luteolin (50 mg/kg *p.o.*) suspended in Na-CMC (0.5% *w/v*); Group Ⅴ: diabetic rats received luteolin (75 mg/kg *p.o.*) suspended in Na-CMC (0.5% *w/v*). The treatment was continued for 8 weeks for all animals, and the body weight of the rats was monitored throughout the experiment. After 8 weeks of luteolin treatment, blood samples were collected from the retro-orbital plexus, and the serum was separated by centrifuging the blood at 7000 rpm for 15 min at 4 ℃. The obtained serum was then tested for blood glucose level, creatinine, blood urea nitrogen (BUN), uric acid, total protein (TP), serum albumin, total cholesterol (TC), and alkaline phosphatase (ALP). Finally, the rats were sacrificed by CO_2 euthanasia, and their kidneys were extracted immediately and preserved for further biochemical studies. A piece of the kidney was also preserved separately in 10% buffered formalin for histopathological evaluation.

2.4. Measurement of biochemical parameters

Fasting blood glucose (FBG), serum creatinine, BUN, uric acid, serum albumin, TC, TP, and ALP[15] were all tested using Erba Diagnostic Kits.

2.5. Renal tissue homogenate preparation

Immediately after sacrifice, both kidneys were removed and thoroughly rinsed with phosphate buffer solution (PBS) to remove excess blood. Each kidney was cut in half. Histopathological analysis was performed on one half. The other half was kept in an ice-cold Petri dish. Thin slices of tissue were cut from the tissues using a surgical scalpel and blotted quickly on filter paper. Using a glass homogenizer, the kidneys were minced before being mixed with 10% (*w/v*) phosphate buffered (pH 7.4). Using the Remi refrigerated centrifuge, 25 strokes of a solid Teflon pestle were used to homogenize the tissue at a speed of 7000 *g* for 20 min at 4 ℃. A clear supernatant obtained was used for the measurement of metalloenzyme (MMP-2, MMP-9, and HDAC-2) levels according to commercial kits and the manufacturer's instructions, as well as for other parameters [malondialdehyde (MDA), myeloperoxidase (MPO), and hydroxyproline (HP)].

2.6. Estimation of antioxidative parameters

Lipid peroxidation was quantified by measuring MDA levels using the thiobarbituric acid reaction technique of Okhawa *et al*. As previously reported, these procedures were standardized in our laboratory[16]. To estimate lipid peroxidation, 0.2 mL of tissue homogenate was combined with 0.2 mL of 8.1% sodium dodecyl sulfate, 1.5 mL of 30% acetic acid (pH 3.5), and 1.5 mL of 0.8% thiobarbituric acid. The reaction mixture was heated at 95 ℃ for 60 min before being cooled on ice. After cooling, 5.0 mL of *n*-butanol:pyridine solution (15:1 *v/v*) was added and centrifuged at 5000 rpm for 20 min. The absorbance of the pink color produced in the organic layer was measured at 532 nm, and the levels of MDA were presented as nM/mg of protein.

2.7. Estimation of MPO activity and HP content in the kidney tissue

The activity of MPO was determined utilizing the previous methodology[16]. In brief, the experimental samples (10 µL) were subjected to a treatment of 80 µL of 0.75 mM H_2O_2 for 5 min at a temperature of 37 ℃, followed by the addition of 3,3′,5,5′-tetramethylbenzidine solution (110 µL). The reaction was subsequently terminated with the addition of 50 µL of 2 M H_2SO_4, and the absorbance was measured spectrophotometrically at a wavelength of 450 nm, in terms of mM H_2O_2 consumed per min per mg of protein. Additionally, the level of HP was determined using Woessner's technique[16]. The levels of MPO and HP were estimated as per a protocol standardized in our laboratory and documented[16].

2.8. Cell culture

NRK-52E, a rat renal proximal tubular cell line, was provided by National Centre for Cell Sciences in Pune, India. The growth medium employed was Dulbecco's modified Eagles medium (Gibco, Life Technologies) supplemented with 10% fetal bovine serum, 100 U/mL penicillin, and 100 g/mL streptomycin, which were

maintained at 37℃ in a humidified atmosphere comprising of 5% CO_2 and 95% air. To ensure optimal cell growth, the culture medium was replaced on alternate days, and subculturing was performed once the confluency reached 75%-80%. To prepare the cells for experimentation, a solution of trypsin-phosphate versine glucose was utilized to separate the cells from the media, following which they were centrifuged and seeded in a growth medium[17]. After a period of 24 h, the cells were seeded and exposed to various conditions, including a blank control (no treatment), normal glucose (5.6 mM), high glucose (30 mM), and high glucose (30 mM) with luteolin at concentrations of 50 μM and 100 μM, for next 48 h. The drugs were dissolved in 1% dimethyl sulfoxide (DMSO) for cell therapy, and strict aseptic conditions were maintained throughout the trial[17].

2.9. MTT assay

To assess the effect of drugs on cell viability, 3-(4,5-dimethylthiazol-2-yl)-2,5-diphenyltetrazolium bromide or methyl thiazolyl tetrazolium (MTT) (Sigma Aldrich) assay was used. The MTT assay is a colorimetric assay used to assess the effect of drugs on cell viability. It involves the reduction of yellow tetrazolium salt to purple formazan crystals in metabolically active cells. In viable cells, NAD(P)H-dependent oxidoreductase enzymes (such as mitochondrial succinate dehydrogenase) convert MTT reagent to formazan, an insoluble crystalline product with a deep purple color. Insoluble formazan crystals are dissolved using DMSO and can be quantitated by measuring absorbance at 570 nm using a spectrophotometric plate reader. The color formation in the solution is directly proportional to the number of viable, metabolically active cells in the solution. After culturing NRK-52E cell lines in 96-well plates, the assay was performed. Briefly, the cells were cultured for 24 h at 37℃ in a 5% CO_2 atmosphere (Thermo Scientific BB150). Then they were treated with different concentrations of luteolin (5, 25, 50, and 100 μM) and incubated for 24 h. At the end of the drug treatment period, the medium was removed from all wells, and the cells were washed with 100 μL of PBS. After washing, the cells received 200 μL of new medium and 20 μL of MTT solution (5 mg/mL in PBS). The plate was covered with aluminum foil for 4 h at 37℃ to keep it dark. After draining the MTT-containing medium, the cells were treated with 200 μL DMSO for 30 min to dissolve formazan crystals. A microplate reader was used to detect absorbance at 550 nm (Benesphera E21). A graph pad prism was used to collect and analyze data, and the percent cell viability was determined[17].

2.10. MMP-2, MMP-9, and HDAC-2 estimation

MMP-2, MMP-9, and HDAC-2 expression were determined in kidney homogenates and cell culture supernatants using a commercial ELISA kit. Rat MMP-2 (gelatinase-A), MMP-9 (gelatinase-B), and HDAC-2 of the GENLISA™ ELISA kits were used according to manufacturer's guidelines. The minimum detection limit for MMP-2, MMP-9, and HDAC-2 was 0.2, 8.0, and 0.1 ng/mL respectively. In terms of variability, the inter- and intra-coefficients of variation for MMP-2 were found to be less than 10% and 8%, respectively; for MMP-9, the coefficients of variation were less than 18% and 15%, respectively; and for HDAC-2, the coefficients of variation were less than 10% and 8%, respectively, in all analyses conducted.

2.11. Histopathological study

The kidneys were carefully removed and stored in a 10% buffered formalin solution before being cut in half along their major axis. Subsequently, they underwent a thorough washing process before being submerged in isopropyl alcohol, xylene, and paraffin for 12 h in preparation for a light microscopic examination. To assess histopathology, 5 μm paraffin-embedded tissue slices were sectioned and stained with hematoxylin and eosin. Abnormalities were noted in glomeruli, tubules, interstitium, and blood vessels. Kidney changes were graded based on neutrophil infiltration and tubular necrosis on a scale where none (-) indicates no necrosis, mild (+) indicates little necrosis, moderate (++) indicates 50% necrotic lesions, and severe (+++) indicates 60% or more necrotic lesions[15].

2.12. Computational studies

Molecular modeling, simulation, and visualization of the protein-ligand complexes were performed using Schrödinger Drug Discovery Suite (Release 2021-1: Schrödinger, LLC, New York, NY, 2021) and Pymol Version 2.4.1.

2.12.1. Ligand and protein preparation

The 2D structure of luteolin was taken from PubChem database[18], and processed using the LigPrep tool of Maestro (Schrödinger Release 2020-4) to generate optimized, low-energy conformer of luteolin using the OPLS3e force field[19]. The specified chirality was retained, and all possible tautomeric states were generated at pH 7.0 ± 2.0 using the Epik[20]. The high-resolution 3D structures of the target proteins were retrieved from the protein data bank (PDB)[21]. The structures of HDAC-2 and MMP-9 (PDB ID: 7KBG and 6ESM)[22,23] were complexed with a co-crystallised inhibitor. The protein structures were incorporated into the maestro workspace and processed by the Protein Preparation Wizard. Briefly, in the pre-processing step, the missing hydrogen atoms were added to the protein structures, and possible het states were generated for co-crystallized ligands using Epik at pH 7.0 ± 2.0. In the next step, the hydrogen bond assignment performed in pre-processing step was optimized using PROPKA at pH 7.0[24]. The water molecules 3 Å away from the ligand were removed, and a restrained minimization was performed using the OPLS3e force field with a convergence criterion of 0.3-Å root-mean-square deviation for all the heavy atoms. The histidine protonation state for zinc binding sites of HDAC-2 and MMP-9 was

given specific attention. The protonation state was optimized using an interactive H-bond optimizer panel using PROPKA at pH 7.0. For HDAC-2 the His141 and His142 were kept delta protonated, whereas His179 was eta protonated. For MMP-9, all three histidine residues (His 226, His 230, and His 236) were kept delta protonated.

2.12.2. Docking protocol

The docking studies were performed using 3D of the co-crystallized ligands. Before the actual docking exercise using the receptor grid generation tool in Maestro, the docking site for HDAC-2 and MMP-9 proteins was defined[25]. The van der Waals scaling factor was kept to a default value of 0.80 with a partial charge limit value of 0.15. To define the grid box for docking, the size of the outer grid box was fixed at 30 Å × 30 Å × 30 Å and the inner grid box dimensions were 10 Å × 10 Å × 10 Å in x, y, z directions. The docking was conducted using the Glide extra precision modes with flexible ligand sampling. The Epik state penalties were added to the final docking scores. For each ligand, ten poses were used for post-docking minimization with a threshold of 0.50 kcal/mol. A maximum of 5 poses per ligand were generated. The docking protocol for HDAC-2 and MMP-9 was validated by redocking the co-crystallized ligands with their respective crystal positions.

2.12.3. Binding free energy estimation

The separated crystallized ligand and protein structures were used to calculate the binding free energy for the co-crystallized ligand complex. To calculate binding free energy for luteolin, the pose viewer file obtained from the Glide extra precision docking was used as an input to calculate binding free energy using Prime MM-GBSA[26], with VSGB2.1[27] as an implicit solvation model and an OPLS3e force field. The binding free energy ΔG_{bind} was calculated using the following equation, as mentioned in our previous protocol[28]:

$$\Delta G_{bind}=\Delta E_{MM}+\Delta G_{solv}+\Delta G_{SA}$$

The Prime/MM-GBSA energies after the molecular dynamics (MD) simulation were calculated from the last 50 ns of the simulation.

2.12.4. MD simulation

The MD simulation was optimized, as previously reported[28]. The MD simulation was performed on HDAC-2 and MMP-9 in a complex with co-crystallized inhibitors and luteolin. Each protein-ligand complex was submitted to a 100-ns MD simulation using Desmond (Schrödinger Release 2020-4: Desmond Molecular Dynamics System, D. E. Shaw Research, New York, NY, USA, 2020)[28]. The simulations helped to refine the poses of luteolin, and its binding affinity could be compared with the native crystal complexes of N-{(1S)-5-[(2-fluoro-6-hydroxybenzene-1-carbonyl) amino]-1-[5-(naphthalen-2-yl)-1H-imidazol-2-yl]pentyl}-1,3-thiazole-5-carboxamide (benzamide inhibitors) and (2~{S})-2-[2-[4-(4-methoxyphenyl)phenyl]sulfanylphenyl]pentanedioic acid (a thioaryl derivative) in complex with HDAC-2 and MMP-9, respectively. The simulation systems were prepared using the System Builder tool. The single-point charge water was chosen as the explicit solvation model[28]. Each system was neutralized using Na^+ or Cl^- as a counter ion. An orthorhombic simulation box, with Periodic Boundary Conditions and a 10-Å buffer space between the solute and the box edge, was defined for each system. The simulation systems were minimized and briefly equilibrated before running production simulations in a stepwise manner. The production simulation was performed using the NPT ensemble for 100 ns, with a reversible reference system propagator algorithm integrator. The temperature (300 K) was set using the Nosé-Hoover chain thermostat, with a relaxation time of 1.0 ps. The pressure was set at 1.013 bar with the Martyna-Tobias-Klein barostat, using isotropic coupling and a relaxation time of 2.0 ps. Long-range interactions were handled using the U-series method; and for short-range interactions, a cut-off radius of 9.0 Å was used. The MD trajectories were analyzed using the Maestro built-in Simulation Interactions Diagram tool and Microsoft Excel 360[28].

2.12.5. Docking validation

We performed validation of docking pose by redocking exercise on co-crystallized ligands at their respective co-crystallized binding site. Figure 1A shows the co-crystallized and redocked pose of the benzamide inhibitor at the HDAC-2 site. The conformation of thiazole ring adopts a slightly different conformation in docked poses when compared to co-crystallized pose but still, the binding free energies of both co-crystallized and redocked poses are almost similar (−30.88 and −30.21 kcal/mol, respectively). Similarly, in Figure 1B, co-crystallized and redocked poses of a thioaryl derivative are compared. The binding free energy of thioaryl derivative in a native co-crystalized pose is −53.77 kcal/mol and in redocked poses, it is −64.19 kcal/mol, which is slightly improved during docking due to better adoption of aromatic hydrogen atoms in the binding site.

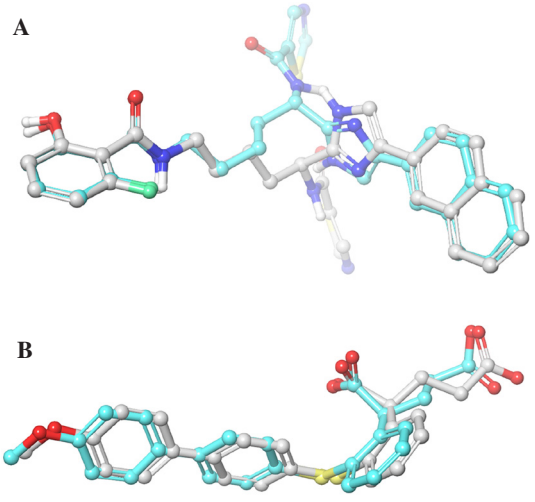

Figure 1. The co-crystallized and redocked poses for (A) benzamide inhibitor at HDAC-2 site and (B) thioaryl derivative at MMP-9 site are shown. The binding site is hidden for clarity, co-crystallized poses are shown in light gray, redocked poses are shown in cyan color ball and stick representation, and non-polar hydrogens are not shown.

2.13. Statistical analysis

Values were expressed as mean ± SEM and statistical analysis was performed using GraphPad Prism (version 6.0 for Windows, GraphPad Software Inc., San Diego, California, USA). One-way ANOVA and Dunnett's test were used for data analysis, with $P < 0.01$ considered statistically significant.

2.14. Ethical statement

All experimental procedures were conducted in accordance with Committee for the Purpose of Control and Supervision of Experiments on Animals, under the Ministry of Social Justice and Empowerment, Government of India. The Institutional Animal Ethics Committee at Dr. M. S. Gosavi College of Pharmaceutical Education and Research, Nashik, approved all animal use and care procedures (Ref. No. MSGCOPER/IAEC/01/2016).

3. Results

3.1. Effect of luteolin on biochemical parameters in renal tissue of STZ-induced diabetic rats

Table 1 presents the results of biochemical parameters following luteolin treatment in STZ-induced diabetic rats. Our results revealed significantly elevated levels of blood glucose, serum creatinine, BUN, TC, ALP, and uric acid in the diabetic control group, along with markedly decreased levels of TP and total albumin, indicating severe impairment in renal function. However, treatment with all doses of luteolin reversed the STZ-induced changes (P<0.01).

3.2. Effect of luteolin on body weight and mortality

At the end of the eighth week, it was observed that the average body weight of the rats in the normal control group had undergone a considerable enhancement. Body weight differences between the diabetic control and non-diabetic rats were found to be statistically significant (P<0.01). However, treatment with luteolin significantly increased body weight at all doses, indicating that luteolin has a beneficial effect on body mass (Table 1).

After one week, the mortality rate in STZ-treated rats was 4.76%. After 2 weeks of STZ injection, the mortality rate in the diabetic control group was 9.52%, while it was 2.38% in the diabetic rats treated with luteolin 25 mg/kg orally. There was no mortality in diabetic rats receiving 50 and 75 mg/kg of luteolin. The all-cause mortality rate in the study was 16.67%.

3.3. Effect of luteolin on MDA, MPO, and HP content in renal homogenate

The levels of MDA in the kidney tissue of rats with streptozotocin-induced diabetes were significantly higher (P<0.01) as compared to non-diabetic rats. Furthermore, administering luteolin at doses of 25, 50, and 75 mg/kg markedly reduced (P<0.01) MDA content in renal tissues of diabetic rats when compared to the diabetic control group. In addition, MPO activity and HP content were significantly elevated (P<0.01) in diabetic control rats when compared to non-diabetic rats. However, luteolin treatment at all doses resulted in a substantial decrease (P<0.01) in MPO activity and HP content in renal tissues, as demonstrated in Table 2.

3.4. Effect of luteolin on the viability of NRK-52E cells treated with high glucose

Exposure to high glucose (30 mM) significantly decreased the viability of renal tubular epithelial cells (NRK-52E) (Figure 2). Treatment with different concentrations of luteolin (5, 25, 50, and 100 μM) under high glucose conditions resulted in a significantly higher percentage of cell viability compared to the high glucose-treated group (P<0.01). Moreover, treatment with luteolin (50 and 100 μM) induced no noticeable changes in cell viability under normal glucose conditions (P>0.05).

Table 1. Effect of luteolin on renal function, blood glucose level, and lipid profile in streptozotocin-induced diabetic rats.

Parameters	Normal	Diabetic control	Luteolin (25 mg/kg)	Luteolin (50 mg/kg)	Luteolin (75 mg/kg)
Body weight (g)	291.0±3.9	151.0±2.8$^{\#}$	194.0±2.7*	193.0±3.6*	213.0±5.2*
Blood glucose level (mg/dL)	119.00±1.55	441.60±9.97$^{\#}$	395.50±4.82*	390.00±7.83*	370.50±5.72*
Serum creatinine (mg/dL)	0.66±0.02	2.19±0.11$^{\#}$	1.31±0.02*	1.34±0.02*	1.25±0.03*
Blood urea nitrogen (mg/dL)	21.38±1.12	52.57±1.62$^{\#}$	37.31±2.67*	25.17±1.25*	28.30±0.89*
Uric acid (mg/dL)	1.57±0.15	4.74±0.22$^{\#}$	2.55±0.08*	2.18±0.09*	2.21±0.05*
Total protein (g/dL)	5.88±0.30	3.74±0.19$^{\#}$	5.92±0.04*	5.89±0.15*	5.80±0.07*
Serum albumin (g/dL)	4.30±0.12	3.10±0.07$^{\#}$	4.70±0.13*	4.70±0.03*	4.80±0.12*
Total cholesterol (mg/dL)	54.60±1.35	192.30±3.10$^{\#}$	131.50±6.80*	134.50±4.20*	128.50±2.70*
Alkaline phosphatase (U/L)	78.67±1.88	204.00±4.78$^{\#}$	124.33±3.36*	97.33±2.45*	104.67±4.04*

Values are expressed as mean ± SEM (n=6) and analyzed using one-way ANOVA and Dunnett's test. $^{\#}P$<0.01 compared with the normal control group, $^{*}P$<0.01 compared with the diabetic control group.

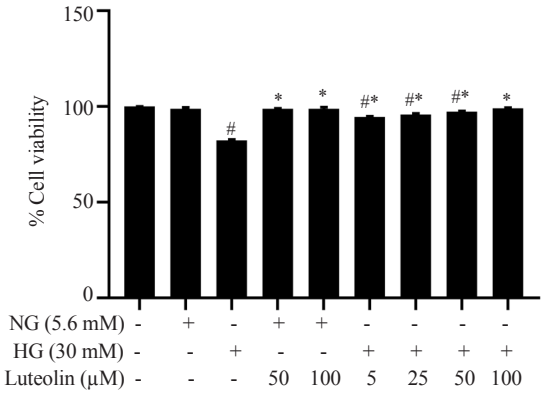

Figure 2. Effect of luteolin on the viability of high glucose-induced NRK-52E cells at 48 h. Cells were incubated with normal glucose (NG, 5.6 mM), normal glucose (5.6 mM) with luteolin (50 and 100 μM), high glucose (HG, 30 mM), and high glucose (30 mM) with luteolin (5, 25, 50, and 100 μM) for 48 h. Data are expressed as mean ± SEM (n=4) and analyzed using one-way ANOVA with Dunnett's test. #represents a significant difference compared with the normal glucose group (P<0.01); *represents a significant difference compared with the high glucose control (P<0.01).

3.5. Effect of luteolin on MMP–2, MMP–9 and HDAC–2 expression in high glucose–induced NRK–52E cells

In accordance with the study protocol, NRK-52E cells were subjected to high glucose treatment in order to investigate the effect of luteolin on the levels of MMP-2, MMP-9, and HDAC-2. As shown in Figure 3A, the levels of MMP-2, MMP-9, and HDAC-2 were significantly increased in NRK-52E cells after high glucose treatment for 48 h, when compared to the normal glucose group. However, administration of 50 and 100 μM of luteolin effectively reversed the high glucose-induced alterations in MMP-2, MMP-9, and HDAC-2 levels, as compared to the high glucose group (P<0.01).

3.6. Effect of luteolin on MMP–2, MMP–9 and HDAC–2 expression in renal tissue of STZ–induced diabetic rats

When compared to the non-diabetic group, MMP-2, MMP-9, and HDAC-2 levels were considerably (P<0.01) higher in the diabetic control group. Treatment with luteolin significantly reduced the expression of MMP-2, MMP-9, and HDAC-2 in the renal tissue of STZ-induced diabetic rats (P<0.01) (Figure 3B).

3.7. Effect of luteolin on morphological changes in the kidney of STZ–induced diabetic rats

The overall pathological abnormalities of the renal tissue were evaluated using hematoxylin and eosin staining. The renal tissues of diabetic control rats showed obvious histological changes, compared with the non-diabetic group which demonstrated an intact renal structure, as depicted in Figure 4. The STZ-induced diabetic group also displayed a considerably higher histological score than the non-diabetic group for aberrant glomerular architecture, infiltration of inflammatory cells (blue arrows), glomerular hyperplasia, alterations in the urinary space, and tubular necrosis of the renal tissue (red arrows). Additionally, an elevated histological grade for tubular fibrosis was shown in the diabetic group. Treatment with 25, 50, and 75 mg/kg of luteolin significantly improved these pathological changes induced by STZ.

3.8. Docking and binding free energy

In order to investigate the interactions between drug molecules and the enzymes HDAC-2 and MMP-9, we conducted docking and binding free energy estimations. The results of these calculations are presented in Table 3, which details the docking score and binding free energy before the implementation of MD simulations, as well as the average binding free energy calculated during the final 50 ns of the MD simulation. Additionally, we compared the docking score to that of the co-crystallized ligand at both the HDAC-2 and MMP-9 sites and evaluated the binding free energy scores in relation to the co-crystallized pose. In our initial docking and binding free energy calculations, we also examined the compounds atorvastatin, kaempferol, and vorinostat in addition to luteolin. However, we did not observe any significant interactions for these compounds at both the HDAC-2 and MMP-9 sites, and thus, they were not considered for further studies.

3.9. MD simulation

To get a detailed understanding of binding affinity and to see the stability of docked poses of luteolin at both the HDAC-2 and MMP-9 sites, we performed a 100-ns long MD simulation. The simulation results were also compared with known inhibitors of HDAC-2 and MMP-9 present in the co-crystallized complex. Supplementary Figure shows the root-mean-square deviation and root-mean-

Table 2. Effect of luteolin on malondialdehyde, myeloperoxidase and hydroxyproline content in streptozotocin-induced diabetic rats.

Parameters	Normal	Diabetic control	Luteolin (25 mg/kg)	Luteolin (50 mg/kg)	Luteolin (75 mg/kg)
Malondialdehyde (nM/mg of protein)	8.19±0.63	85.25±2.07#	17.89±0.69*	13.04±0.31*	12.84±0.76*
Myeloperoxidase (μM/mg of protein)	18.60±0.79	51.48±2.07#	20.19±1.72*	18.65±1.43*	17.13±0.82*
Hydroxyproline (μg/mg of protein)	4.49±0.37	9.09±0.22#	4.62±0.21*	4.24±0.15*	4.48±0.20*

Values are expressed as mean ± SEM (n=6) and analyzed using one-way ANOVA with Dunnett's test. #P<0.01 compared with the normal control group, *P<0.01 compared with the diabetic control group.

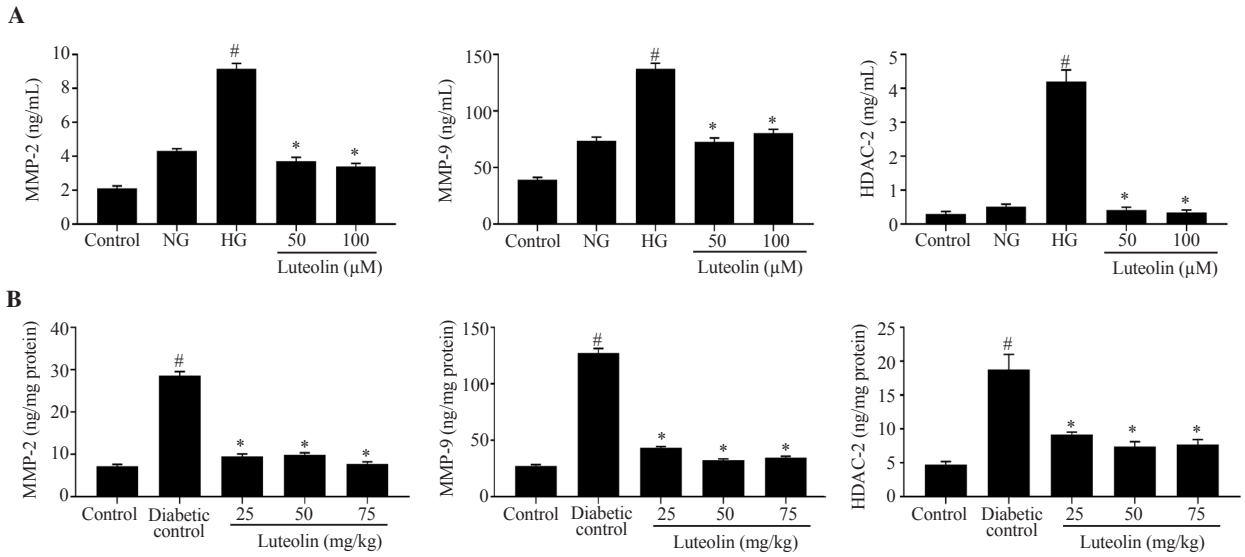

Figure 3. Effect of luteolin on MMP-2, MMP-9, and HDAC-2 expression in (A) NRK-52E cells under high glucose conditions and (B) in the kidney tissue of STZ induced diabetic rats. Data are expressed as mean±SEM (n=6) and analyzed using one-way ANOVA with Dunnett's test. #represents a significant difference compared to the normal glucose group or the normal control group (P<0.01); *represents a significant difference compared to the high glucose group or the diabetic control group (P<0.01).

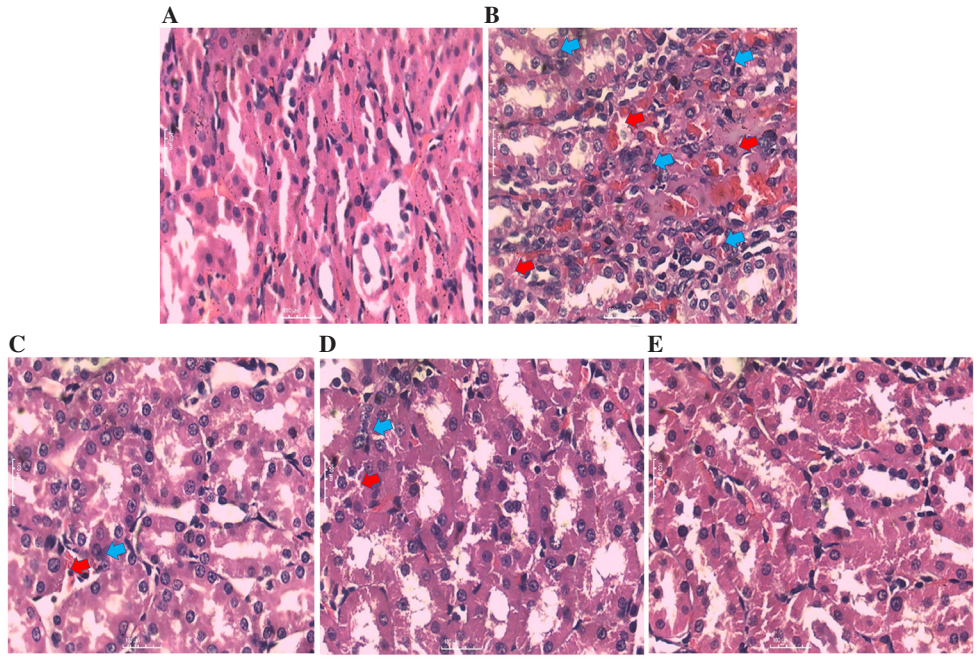

Figure 4. Representative images of hematoxylin and eosin (H&E) stained kidney section under light microscopy at 100× magnification. (A) The normal group shows normal architecture of kidney; (B) the diabetic control group shows severe neutrophil infiltration (blue arrow) and tubular necrosis (red arrow); (C) the diabetic group treated with 25 mg/kg luteolin shows mild or none neutrophil infiltration and tubular changes; (D) the diabetic group treated with 50 mg/kg luteolin shows no or mild neutrophil infiltration and tubular changes; (E) the diabetic group treated with 75 mg/kg luteolin shows normal architecture of kidney and histology. Blue arrow: infiltration of neutrophils; red arrow: tubular changes.

Table 3. Docking scores and binding free energy estimation at HDAC-2 and MMP-9 sites.

Compounds	HDAC-2 site			MMP-9 site		
	Docking score	MMGBSA before MD (kcal/mol)	Average MMGBSA calculated from last 50 ns of MD simulation (kcal/mol)	Docking score	MMGBSA before MD (kcal/mol)	Average MMGBSA calculated from last 50 ns of MD simulation (kcal/mol)
Redocked/co-crystallized ligand	−12.290	−30.21	−24.65	−13.340	−64.19	−55.61
Atorvastatin	−5.550	11.06		−8.015	9.38	-
Luteolin	−5.390	−22.88	−21.29	−7.870	−39.76	−36.55
Kaempferol	−5.720	−16.15	-	−4.857	14.75	-
Vorinostat	−9.804	−15.44	-	−8.274	−28.43	-

The binding free energy values are representative only and do not reflect experimental affinities of these compounds. MD: molecular dynamics.

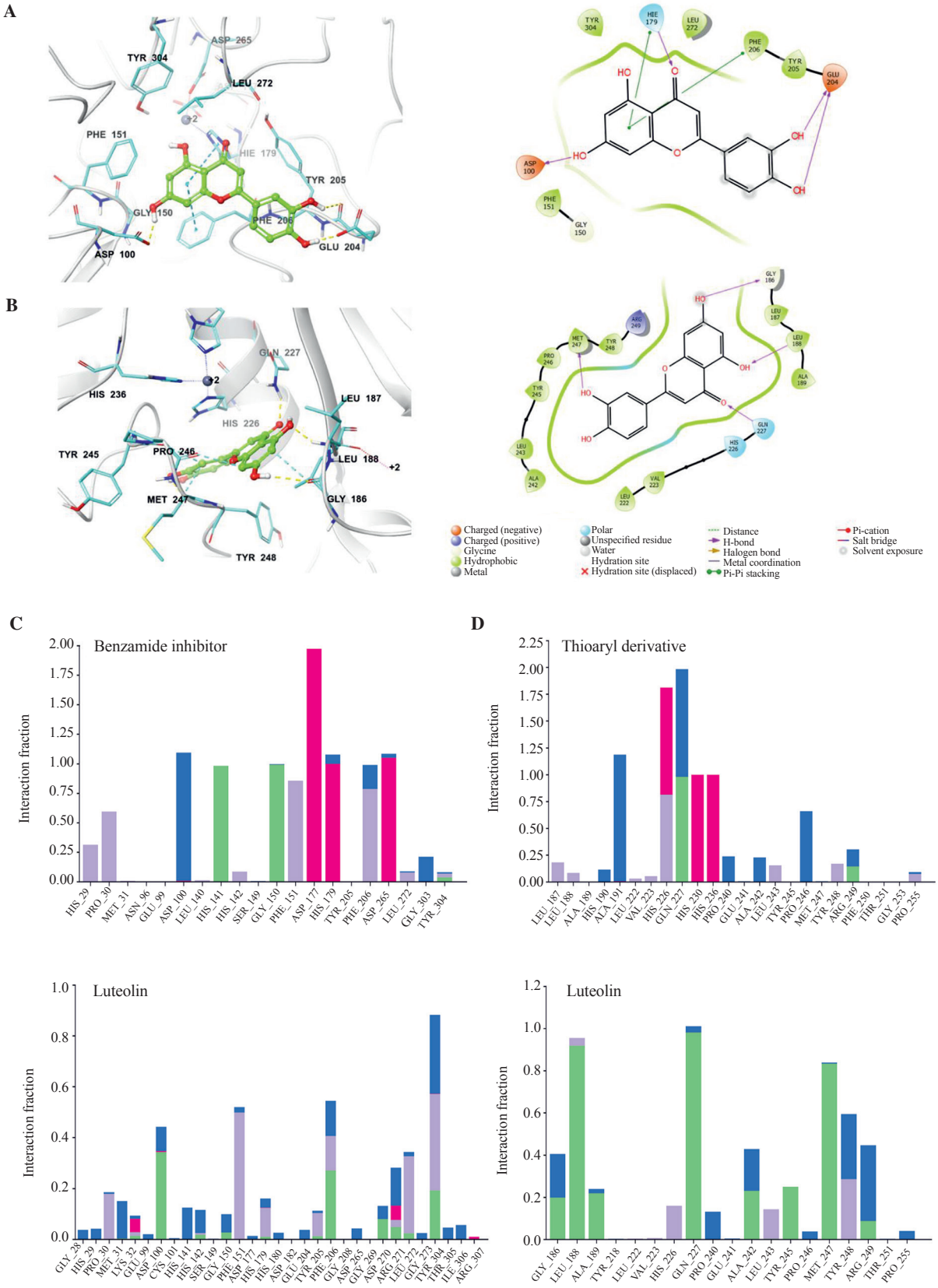

Figure 5. The docked poses of luteolin at (A) HDAC-2 and (B) MMP-9 binding sites in 3D (left panel); protein chains in light gray cartoon; key interacting residues in cyan sticks; Zn^{2+} ion shown as a gray sphere; interactions as dashed lines; color of interaction type: yellow—hydrogen bonds; green—pi-cation interaction; cyan—pi-pi stacking; dark pink—salt bridge; magenta–halogen bond and in 2D (right panel). (C) The interaction pattern of the benzamide inhibitor and luteolin at the HDAC-2 site. (D) The interaction pattern of thioaryl derivative and luteolin at the MMP-9 site. The stacked bar charts are normalized throughout a 100-ns MD simulation; the interaction fraction value indicates how long the interaction lasted for simulation time. Color code: green–hydrogen bond interactions, blue–water-mediated interactions, purple-hydrophobic interactions, red–ionic interactions. Only interactions with amino acid residues are shown.

square fluctuation graphs of luteolin with benzamide and thioaryl derivatives. The root-mean-square deviation of HDAC-2 and MMP-2 was well stabilized by luteolin when compared with co-crystallized inhibitors. Similarly, the root-mean-square fluctuation values remained low for both proteins in the presence of docked luteolin. However, luteolin lost contact with Phe206 after 70 ns which caused a little increase in root mean-square fluctuation at this position. Figure 5 illustrates the docked poses of luteolin at the binding sites of both HDAC-2 and MMP-9. It also signifies the interaction pattern of the benzamide inhibitor at HDAC-2 with luteolin, as well as the thioryl derivative at the MMP-9 site with luteolin.

4. Discussion

Diabetes complications are a global public health concern due to their high prevalence, significant social and economic impact, and life-threatening morbidity. Despite their fatal nature, they are difficult to prevent due to the lack of effective treatment options. Therefore, there is an urgent need for new pharmacological agents to combat the risk of diabetes. Recent studies have investigated natural products as potential renoprotective drugs by suppressing renal oxidative stress, inflammation, and fibrosis in the early stage of experimental DN[29] The focus of our study has been on using new approaches such as structure-based drug design and MD simulations to study the interactions of luteolin, a flavonoid compound, with HDAC-2 and MMPs. These two proteins play a critical role in the progression of diabetes, and thus, we have employed a variety of biochemical, *in vivo*, and *in vitro* analysis methods to assess the beneficial effects of luteolin on these proteins.

Collagen Ⅳ is the primary component of the glomerular basement membrane and ECM in the kidneys, and proteinuria results from glomerular structural alterations caused by abnormal ECM accumulation and degradation. MMPs play a crucial role in this pathophysiological process[5]. Studies have shown that chronic use of specific MMP inhibitors may slow the progression and potentially cure hypertension and DN[4]. Additionally, previous research has shown that MMP-2 and MMP-9 levels increase in diabetic rats after the administration of STZ. Inhibition of these enzymes in the presence of a cyclooxygenase inhibitor has been shown to prevent the development of experimental DN[5]. Furthermore, overexpression of MMP-9 has been linked to the dedifferentiation of podocytes, which leads to albuminuria and ECM protein production, ultimately resulting in the development of DN in both experimental models and in diabetic patients. Conversely, MMP-9 deficiency in diabetic mice has been shown to alleviate the disease[6]. In diabetic kidneys, HDAC-2 plays a crucial role in the development of ECM and EMT, and ROS facilitates TGF-β-1-induced activation of HDAC-2[8]. HDAC-2 activity was significantly increased in STZ-induced diabetic rats, db/db mice, and NRK-52E cells exposed to TGF-β-1, confirming the role of HDAC-2 in renal fibrosis. Furthermore, treatment with the HDACs inhibitor Trichostatin A (TSA) or HDAC-2 knockdown alleviates the TGF-β-1-induced EMT in NRK-52E cells[8]. It was evident from previous research that luteolin suppresses HDAC-2. Inhibition of HDACs may play a role in this phenomenon by indirectly increasing acetylation levels. Consequently, this cascade of events may potentially trigger the activation of diverse genes, including caspases[30]. In another cell experiment, luteolin had a positive effect on cell viability and reduced apoptosis by inhibiting MMP-9 and activating the PI3K/Akt signaling pathway in ischemia stroke[31]. In our study, the expression of MMP-2, MMP-9, and HDAC-2 was significantly increased in the diabetic control group. After treatment with the flavonoid luteolin, the expressions of MMP-2, MMP-9, and HDAC-2 were decreased suggesting that early treatment with luteolin may have a potent inhibitory effect on these enzymes in DN.

The utilization of *in vitro* models has recently gained widespread acceptance due to their ease of use and ability to analyze a multitude of aspects related to the development of disease without external hindrances. The NRK-52E cell line is widely used in renal system and DN research, investigating the compound's renal toxicity and renal diseases[17]. Oxidative stress and inflammation significantly contribute to the development and progression of DN and chronic kidney disease (CKD). These effects happen in a cycle where oxidative stress causes inflammation through different mechanisms that create ROS, activate leukocytes, and cause more oxidative stress[17,32].

High glucose (30 mmol/L) causes considerable damage to renal tubular epithelial cells (NRK-52E) *via* the generation of ROS that enhance oxidative stress and trigger apoptosis[32]. Furthermore, TGF-β-1 expression is induced by high glucose, which leads to the overproduction of MMP-2, MMP-9, and ECM proteins in NRK-52E cells[33], hence expanding their size[34]. MMP-2 and MMP-9 expressions are linked with hyperglycemia and enhanced in response to glucose[34]. High glucose also induces inflammatory cytokines and fibrogenic responses, leading to NRK-52E cell injury; however, flavonoids have been shown to possess antioxidant and anti-inflammatory effects that alleviate renal injury[35]. High glucose enhances the expression and activity of the HDAC-2 enzyme by inducing apoptosis through oxidative stress[36]. In the current study, our results showed that high glucose conditions affected cell viability compared to normal glucose. Moreover, high glucose conditions did increase the expression and levels of the enzymes MMP-2 and MMP-9, as well as HDAC-2, which is in accordance with the aforementioned studies. In addition, luteolin treatment increased the survival of NRK-52E cells in a dose-dependent way, as

well as inhibited the MMPs and HDAC-2 levels under high glucose conditions.

We also investigated the impact of luteolin on kidney impairment in STZ-induced diabetic rats, a widely used model for studying early modifications in diabetic kidneys. STZ targets and destroys Langerhans islets, making it a commonly used method for causing experimental kidney damage[37]. Persistent hyperglycemia and poor blood pressure control are risk factors for the initiation and progression of DN. Diabetic rats experience deterioration of the typical diabetes triad, polyuria, polydipsia, and polyphagia when glucose level increases[37]. The hypoglycemic and antioxidant properties of luteolin have been found to protect the pancreas and promote insulin secretion, making it a valuable and significant subject for medical research[38]. Luteolin has been shown to possess anti-diabetic actions that improve blood glucose levels, HbA1c levels, and insulin levels, and inhibit lipid synthesis[39]. In the current investigation, blood glucose levels in diabetic rats were increased significantly after treatment with STZ, however, luteolin treatment significantly reduced hyperglycemia in the diabetic rats, which may be partly attributed to its ability to regenerate or repair residual cells, thus increasing insulin secretion.

The body weight of diabetic rats is significantly reduced as a result of excessive breakdown of tissue proteins[37]. In the current study, treating diabetic rats with luteolin resulted in a significant improvement in body weight, indicating the prevention of hyperglycemia-related damage to muscle tissue.

Progression of disease is attributed to consistent hyperglycemia and increased levels of serum creatinine, BUN, and uric acid, as shown in the present study in STZ-diabetic rats. This finding aligns with previous experimental investigations in diabetic rats, referring to progressive renal damage[5,15]. TP and albumin in the blood decrease while renal parameters increase. A decrease in serum albumin is clinically associated with poor renal prognosis and reduced kidney function in DN[40]. In our study, administration of luteolin at different doses (25, 50, and 75 mg/kg) markedly reduced the levels of serum creatinine, BUN, ALP, TC, and uric acid, while increasing TP and albumin levels, indicating an improvement in renal function and enhanced renal health in diabetic rats. Similar findings were reported regarding the renoprotective effect of luteolin[13,38].

The underlying cause of the onset and progression of DN is hyperglycemia, which leads to renal dysfunction triggered by the overproduction of ROS. Oxidative stress and uncontrolled ROS formation trigger the initiation and exacerbation of various disease-related processes[15]. In our study, we observed increased levels of MDA, the end product of lipid peroxidation, MPO, a marker used to evaluate neutrophil infiltration, and HP, which is known to contribute to the severity of fibrosis in the renal tissue of diabetic rats. In the present study, treatment with luteolin effectively reduced oxidative stress, MPO, and HP levels in the renal homogenate of diabetic rats; these results support previous researches[13,15,37], suggesting the antioxidant and anti-inflammatory properties of luteolin may play a crucial role in the prevention of DN.

Histopathological investigations revealed that diabetic animals sustained damage to their renal cells and more than half of the morphological changes in tubular cells were observed, such as swelling, necrosis, and medullary congestion. The glomerular architecture was maintained in the rat kidneys treated with luteolin (at doses of 25, 50, and 75 mg/kg), however, there were anomalies present in the urinary tract, including glomerular hyperplasia, inflammatory cell infiltration, and tubular edema of renal tissue. The kidneys of STZ-induced diabetic rats displayed severe tubular fibrosis. Luteolin therapy could reduce STZ-induced renal fibrosis in a dose-dependent manner. These findings align with previous studies in which chronic administration of selective MMP inhibitors improved renal histology and had the potential to slow the progression of DN as MMP activation may play a significant role in the development of glomerulosclerosis, tubular atrophy, and interstitial fibrosis in hypertension- and diabetic-induced nephropathy[4,8].

In our computational studies, we observed robust binding of luteolin with HDAC-2 and MMP-9. The docked poses of luteolin at both HDAC-2 and MMP-9 binding sites were found. At the HDAC-2 site, luteolin showed strong hydrogen bonding interactions, which can be seen in interactions with Asp100, Glu204, and His179 residues. Both His179 and Phe206 showed pi-pi stacking interactions with the aromatic ring of luteolin. The docking of luteolin at the MMP-9 site demonstrated strong hydrogen bonding interactions with Gly186, Leu188, Gln227, and Met247, and aromatic hydrogen bond interactions with Gly186 and Pro246 residues. The HDAC-2 enzyme is known to exhibit two distinct states of zinc coordination, namely a tetrahedral or penta-coordinated trigonal bipyramidal state, depending on the occupation of the binding site. These states are representative of the possible mono- or bidentate chelation with zinc-binding groups[41,42]. In contrast, the MMP-9 enzyme contains two Zn^{+2} atoms, one at the catalytic site and the other at the structural site. The catalytic Zn^{+2} ion is situated in the active site of the enzyme and is tetrahedrally coordinated by three histidine side chains. The fourth ligand is the side chain of Cys, the single cysteine residue in the propeptide. In catalytic sites of zinc enzymes, the metal serves to activate a nonprotein ligand or a protein ligand, such as the sulfur donor of cysteine. Due to the presence of steric constraints in providing space for substrate binding in enzymes, the zinc ion often only has three protein ligands, an exchangeable water molecule, and/or a position for coordination of another ligand[43–45]. The structure of HDAC-2 has been co-crystallized with a 2-hydroxy benzamide derivative, also in relation to HDAC-1 and 3. The phenol oxygen

and the benzamide carbonyl chelate the zinc ion in a bidentate mode with prominent ionic interactions with Asp177, His179, and Asp265. Furthermore, hydrophobic interactions with Phe151, Phe206, and hydrogen bonding with His141 and Gly150 are also observed. Additionally, there are water-mediated interactions with Asp100. When these interactions are compared to those of luteolin, strong hydrophobic and hydrogen bond interactions with Phe151, Thr304, Asp100, and Phe206, along with water-mediated interactions, are observed. Similarly, at MMP-9 site, luteolin shows strong hydrogen bond interactions with Leu188, Gln227, and Met247. There are also a few water-mediated and hydrophobic interactions observed at the binding site. Overall, at both sites, luteolin binds and shows stable interactions like co-crystallized inhibitors, giving a strong indication of subsequent inhibition of HDAC-2 as well as MMP-9 inhibition.

To assess the therapeutic potential of luteolin, we examined its effects on kidney damage in STZ-induced diabetic rats by measuring the expression of the enzymes MMP-2, MMP-9, and HDAC-2. A significant increase in MMP-2, MMP-9, and HDAC-2 enzymes was found in the renal tissues of diabetic rats, but luteolin therapy alleviated this increase. Moreover, our computational study confirmed interactions of luteolin at the HDAC-2 and MMP-9 sites during MD simulations. This backs up the MMGBSA analysis's prediction that there will be significant binding free energy. Notably, luteolin retains interactions with amino acids at both sites, which likely play a pivotal role in its ability to inhibit MMP-9 and HDAC-2. These underscore their importance as factors influencing the biological effectiveness of luteolin. Our finding indicates that luteolin could be a potential therapeutic agent by targeting the enzymes MMP-2, MMP-9, and HDAC-2 in DN. Luteolin reduces hyperglycemia and improves renal function, which may be through inhibition of MMP-2, MMP-9, and HDAC-2, as well as inhibition of oxidative stress, inflammation, and fibrosis.

In summary, luteolin mitigates STZ-induced renal damage by inhibiting MMP-2, MMP-9, and HDAC expression, decreasing oxidative stress and inflammation, as well as regulating hyperglycemia, which improves overall renal function. However, further studies are warranted to examine the impact of luteolin on specific signaling pathways in DN.

Conflict of interest statement

The authors declare that they have no conflicts of interest.

Acknowledgments

The authors concede the support by the G.E. S's Sir Dr. M. S. Gosavi College of Pharmaceutical Education and Research Nashik; Institute of Pharmacy, Nirma University, Ahmedabad; and Government Polytechnic, Jalgaon. The Sigrid Jusélius Foundation, Biocenter Finland Bioinformatics and Drug Discovery and Chemical Biology networks, CSC IT Center for Science, Joe, Pentti and Tor Borg Memorial Fund, and Prof. Mark Johnson and Dr. Jukka Lehtonen are gratefully acknowledged for the excellent computational infrastructure at the Åbo Akademi University. We would also like to thank Dr. Outi M. H. Salo-Ahen for constructive feedback on the computational part.

Funding

The study was supported by the Joe, Pentti, and Tor Borg Memorial Fund.

Data availability statement

The data supporting the findings of this study are available from the corresponding authors upon request.

Authors' contributions

RB performed the modeling, MD simulations, and data analysis, as well as wrote the computational portion of the work. RD carried out experiments, gathered and assessed the literature, and wrote the article. JS was in charge of supervising and revising the text. The final manuscript was reviewed and approved by all authors.

References

[1] Wang F, Sun H, Zuo B, Shi K, Zhang X, Zhang C, et al. Metformin attenuates renal tubulointerstitial fibrosis *via* upgrading autophagy in the early stage of diabetic nephropathy. *Sci Rep* 2021; **11**(1). doi:10.1038/s41598-021-95827-5.

[2] DeFronzo RA, Reeves WB, Awad AS. Pathophysiology of diabetic kidney disease: Impact of SGLT2 inhibitors. *Nat Rev Nephrol* 2021; **17**(5): 319-334. doi: 10.1038/s41581-021-00393-8.

[3] Cabral-Pacheco GA, Garza-Veloz I, Rosa CCD La, Ramirez-Acuña JM, Perez-Romero BA, Guerrero-Rodriguez JF, et al. The roles of matrix metalloproteinases and their inhibitors in human diseases. *Int J Mol Sci* 2020; **21**(24): 1-53.

[4] Wozniak J, Floege J, Ostendorf T, Ludwig A. Key metalloproteinase-mediated pathways in the kidney. *Nat Rev Nephrol* 2021; **17**(8): 513-527.

doi: 10.1038/s41581-021-00415-5.

[5] Kumar Bhatt L, Addepalli V. Minocycline with aspirin: An approach to attenuate diabetic nephropathy in rats. *Ren Fail* 2011; **33**(1): 72-78.

[6] Li SY, Huang PH, Yang AH, Tarng DC, Yang WC, Lin CC, et al. Matrix metalloproteinase-9 deficiency attenuates diabetic nephropathy by modulation of podocyte functions and dedifferentiation. *Kidney Int* 2014; **86**(2): 358-369.

[7] Dewanjee S, Vallamkondu J, Kalra RS, Chakraborty P, Gangopadhyay M, Sahu R, et al. The emerging role of HDACs: Pathology and therapeutic targets in diabetes mellitus. *Cells* 2021; **10**(6): 1340.

[8] Noh H, Oh EY, Seo JY, Yu MR, Kim YO, Ha H, et al. Histone deacetylase-2 is a key regulator of diabetes-and transforming growth factor-1-induced renal injury. *Am J Physiol Renal Physiol* 2009; **297**: 729-739.

[9] Ali MM, Mahmoud AM, Le Master E, Levitan I, Phillips SA. Role of matrix metalloproteinases and histone deacetylase in oxidative stress-induced degradation of the endothelial glycocalyx. *Am J Physiol Heart Circ Physiol* 2019; **316**: 647-663.

[10]Aziz N, Kim MY, Cho JY. Anti-inflammatory effects of luteolin: A review of *in vitro*, *in vivo*, and *in silico* studies. *J Ethnopharmacol* 2018; **225**: 342-358. doi: 10.1016/j.jep.2018.05.019.

[11]Xiong C, Wu Q, Fang M, Li H, Chen B, Chi T. Protective effects of luteolin on nephrotoxicity induced by long-term hyperglycaemia in rats. *J Int Med Res* 2020; **48**(4). doi: 10.1177/0300060520903642.

[12]Zhang M, He L, Liu J, Zhou L. Luteolin attenuates diabetic nephropathy through suppressing inflammatory response and oxidative stress by inhibiting STAT3 pathway. *Exp Clin Endocrinol Diabetes* 2021; **129**(10): 729-739. doi: 10.1055/a-0998-7985.

[13]Wang GG, Lu XH, Li W, Zhao X, Zhang C. Protective effects of luteolin on diabetic nephropathy in STZ-induced diabetic rats. *Evid Based Complement Alternat Med* 2011. doi: 10.1155/2011/323171.

[14]Salo-Ahen OMH, Alanko I, Bhadane R, Bonvin AMJJ, Vargas Honorato R, Hossain S, et al. Molecular dynamics simulations in drug discovery and pharmaceutical development. *Processes* 2021; **9**(1): 71. doi: 10.3390/pr9010071.

[15]Chowdhury S, Ghosh S, Das AK, Sil PC. Ferulic acid protects hyperglycemia-induced kidney damage by regulating oxidative insult, inflammation and autophagy. *Front Pharmacol* 2019; **10**(2). doi: 10.3389/fphar.2019.00027.

[16]Daude RB, Shah JS. Protective effect of alpha-cyperone in renal ischemia-reperfusion induced acute kidney injury by modulation of metalloenzyme expression. *Eur Chem Bull* 2023; **12**(Special issue 4): 5629-5643.

[17]Sharma D, Gondaliya P, Tiwari V, Kalia K. Kaempferol attenuates diabetic nephropathy by inhibiting RhoA/Rho-kinase mediated inflammatory signalling. *Biomed Pharmacother* 2019; **109**: 1610-1619. doi: 10.1016/j.biopha.2018.10.195.

[18]Kim S, Chen J, Cheng T, Gindulyte A, He J, He S, et al. PubChem in 2021: New data content and improved web interfaces. *Nucleic Acids Res* 2021; **49**. doi: 10.1093/nar/gkaa971.

[19]Roos K, Wu C, Damm W, Reboul M, Stevenson JM, Lu C, et al. OPLS3e: Extending force field coverage for drug-like small molecules. *J Chem Theory Comput* 2019; **15**(3): 1863-1874.

[20]Bochevarov AD, Watson MA, Greenwood JR, Philipp DM. Multiconformation, density functional theory-based pKa prediction in application to large, flexible organic molecules with diverse functional groups. *J Chem Theory Comput* 2016; **12**(12). doi: 10.1021/acs.jctc.6b00805.

[21]Berman HM, Battistuz T, Bhat TN, Bluhm WF, Bourne PE, Burkhardt K, et al. The protein data bank. *Acta Crystallogr D Biol Crystallogr* 2002; **58**: 899-907. doi: 10.1107/S0907444902003451.

[22]Nuti E, Cuffaro D, Bernardini E, Camodeca C, Panelli L, Chaves S, et al. Development of thioaryl-based matrix metalloproteinase-12 inhibitors with alternative zinc-binding groups: Synthesis, potentiometric, NMR, and crystallographic studies. *J Med Chem* 2018; **61**(10). doi: 10.1021/acs.jmedchem.8b00096.

[23]Liu J, Yu Y, Kelly J, Sha D, Alhassan AB, Yu W, et al. Discovery of highly selective and potent HDAC3 inhibitors based on a 2-substituted benzamide zinc binding group. *ACS Med Chem Lett* 2020; **11**(12). doi: 10.1021/acsmedchemlett.0c00462.

[24]Olsson MHM, SØndergaard CR, Rostkowski M, Jensen JH. PROPKA3: Consistent treatment of internal and surface residues in empirical pKa predictions. *J Chem Theory Comput* 2011; **7**(2): 525-537.

[25]Friesner RA, Murphy RB, Repasky MP, Frye LL, Greenwood JR, Halgren TA, et al. Extra precision glide: Docking and scoring incorporating a model of hydrophobic enclosure for protein-ligand complexes. *J Med Chem* 2006; **49**(21). doi:10.1021/jm051256o.

[26]Jacobson MP, Pincus DL, Rapp CS, Day TJF, Honig B, Shaw DE, et al. A hierarchical approach to all-atom protein loop prediction. *Proteins* 2004; **55**(2): 351-367. doi: 10.1002/prot.10613.

[27]Li J, Abel R, Zhu K, Cao Y, Zhao S, Friesner RA. The VSGB 2.0 model: A next generation energy model for high resolution protein structure modeling. *Proteins* 2011; **79**(10). doi: 10.1002/prot.23106.

[28]Mishra GP, Bhadane RN, Panigrahi D, Amawi HA, Asbhy CR, Tiwari AK. The interaction of the bioflavonoids with five SARS-CoV-2 proteins targets: An *in silico* study. *Comput Biol Med* 2021; **134**. doi: 10.1016/j.compbiomed.2021.104464.

[29]Ruttiya T, Laddawan S, Wiphawi H, Panot T, Patchareewan P. Anti-angiogenesis and anti-inflammatory effects of *Moringa oleifera* leaf extract in the early stages of streptozotocin-induced diabetic nephropathy in rats. *Asian Pac J Trop Biomed* 2022; **12**(7): 290-299.

[30]Domitrović R, Cvijanović O, Pugel EP, Zagorac GB, Mahmutefendić H, Škoda M. Luteolin ameliorates cisplatin-induced nephrotoxicity in mice through inhibition of platinum accumulation, inflammation and apoptosis in the kidney. *Toxicology* 2013; **310**: 115-123.

[31]Luo S, Li H, Mo Z, Lei J, Zhu L, Huang Y, et al. Connectivity map

identifies luteolin as a treatment option of ischemic stroke by inhibiting MMP9 and activation of the PI3K/Akt signaling pathway. *Exp Mol Med* 2019; **51**(3). doi: 10.1038/s12276-019-0229-z.

[32]Tong Y, Liu S, Gong R, Zhong L, Duan X, Zhu Y. Ethyl vanillin protects against kidney injury in diabetic nephropathy by inhibiting oxidative stress and apoptosis. *Oxid Med Cell Longev* 2019; **2019**. doi: 10.1155/2019/2129350.

[33]Strutz F, Zeisberg M, Ziyadeh FN, Yang CQ, Kalluri R, Müller GA, et al. Role of basic fibroblast growth factor-2 in epithelial-mesenchymal transformation. *Kidney Int* 2002; **61**(5): 1714-1728.

[34]Wu L, Derynck R. Essential role of TGF-β signaling in glucose-induced cell hypertrophy. *Dev Cell* 2009; **17**(1): 35-48.

[35]Hu Q, Qu C, Xiao X, Zhang W, Jiang Y, Wu Z, et al. Flavonoids on diabetic nephropathy: Advances and therapeutic opportunities. *Chin Med* 2021; **16**(1). doi: 10.1186/S13020-021-00485-4.

[36]Du Y, Tang G, Yuan W. Suppression of HDAC2 by sodium butyrate alleviates apoptosis of kidney cells in db/db mice and HG-induced NRK-52E cells. *Int J Mol Med* 2020; **45**(1): 210-222.

[37]Ghule AE, Jadhav SS, Bodhankar SL. Trigonelline ameliorates diabetic hypertensive nephropathy by suppression of oxidative stress in kidney and reduction in renal cell apoptosis and fibrosis in streptozotocin induced neonatal diabetic (nSTZ) rats. *Int Immunopharmacol* 2012; **14**(4): 740-748.

[38]Zhang Y, Tian XQ, Song XX, Ge JP, Xu YC. Luteolin protect against diabetic cardiomyopathy in rat model *via* regulating the AKT/GSK-3β signalling pathway. *Biomed Res* 2017; **28**(3): 1359-1363.

[39]Zang Y, Igarashi K, Li YL. Anti-diabetic effects of luteolin and luteolin-7-*O*-glucoside on KK-Ay mice. *Biosci Biotechnol Biochem* 2016; **80**(8): 1580-1586.

[40]Ezzat SM, Abdallah HMI, Yassen NN, Radwan RA, Mostafa ES, Salama MM, et al. Phenolics from *Physalis peruviana* fruits ameliorate streptozotocin-induced diabetes and diabetic nephropathy in rats *via* induction of autophagy and apoptosis regression. *Biomed Pharmacother* 2021; **142**. doi: 10.1016/j.biopha.2021.111948.

[41]Laitaoja M, Valjakka J, Jänis J. Zinc coordination spheres in protein structures. *Inorg Chem* 2013; **52**(19). doi: 10.1021/ic401072d.

[42]Stolfa DA, Marek M, Lancelot J, Hauser AT, Walter A, Leproult E, et al. Molecular basis for the antiparasitic activity of a mercaptoacetamide derivative that inhibits histone deacetylase 8 (HDAC8) from the human pathogen schistosoma mansoni. *J Mol Biol* 2014; **426**(20). doi: 10.1016/j.jmb.2014.03.007.

[43]Pace NJ, Weerapana E. Zinc-binding cysteines: Diverse functions and structural motifs. *Biomolecules* 2014; **4**(2). doi: 10.3390/biom4020419.

[44]Rowsell S, Hawtin P, Minshull CA, Jepson H, Brockbank SMV, Barratt DG, et al. Crystal structure of human MMP9 in complex with a reverse hydroxamate inhibitor. *J Mol Biol* 2002; **319**(1). doi: 10.1016/S0022-2836(02)00262-0.

[45]Yano H, Nishimiya D, Kawaguchi Y, Tamura M, Hashimoto R. Discovery of potent and specific inhibitors targeting the active site of MMP-9 from the engineered SPINK2 library. *PLoS One* 2020; **15**(12). doi: 10.1371/journal.pone.0244656.

Publisher's note